Mon. Not. R. Astron. Soc. (1992) **259**, 67–81

Optical spectroscopy of the *ROSAT* X-ray brightest clusters

S. W. Allen,[1] A. C. Edge,[1] A. C. Fabian,[1] H. Böhringer,[2] C. S. Crawford,[1] H. Ebeling,[2] R. M. Johnstone,[1] T. Naylor[1,3] and R. A. Schwarz[2]

[1] *Institute of Astronomy, Madingley Road, Cambridge CB3 0HA*
[2] *Max-Planck-Institut für extraterrestrische Physik, W-8046 Garching b. München, Germany*
[3] *Department of Physics, Keele University, Keele, Staffordshire ST5 5BG*

Accepted 1992 April 28. Received 1992 April 27; in original form 1992 March 12

ABSTRACT

We present the results from the first stage of an optical follow-up study of the X-ray brightest clusters of galaxies detected in the *ROSAT* All-Sky Survey (RASS). The redshifts of the central galaxies in 29 of the X-ray brightest Abell and Zwicky clusters in the RASS have been measured using the Faint Object Spectrograph on the Isaac Newton Telescope. Approximately 40 per cent of the central galaxy spectra obtained show strong optical line emission. In several cases this emission is quite spectacular. The central cluster galaxy in Zwicky 3146 is the most luminous such galaxy in optical lines yet discovered, having an Hα luminosity approximately twice that of NGC 1275. We re-examine the link between optical line emission and the presence of an excess of blue continuum flux in the spectra and find that the two are correlated. The spectral shape of the excess flux is well matched by B stars.

Key words: surveys – galaxies: clustering – cooling flows – galaxies: elliptical and lenticular, cD – galaxies: stellar content – X-rays: galaxies.

1 INTRODUCTION

Clusters of galaxies are the largest gravitationally bound systems in the Universe, and an understanding of their spatial distribution and evolution is of fundamental importance to cosmological studies. Until recently, the only method for the identification and classification of clusters has been the subjective one of inspecting optical survey plates. Unfortunately, this technique is prone to problems of misidentification and contamination in which physically unassociated foreground and background galaxies are associated with particular clusters through projection effects (Abell 1958; Lucey 1983; Sutherland 1988; Abell, Corwin & Olowin 1989). However, clusters of galaxies are also luminous X-ray sources due to the large quantities of hot, virialized gas trapped deep in their gravitational potential wells. (For a full review of the X-ray properties of clusters of galaxies, see Sarazin 1988.) Since the X-ray emission is proportional to the square of the gas density, which traces the cluster potential (and is therefore highly peaked), it is little affected by projection effects and is an ideal tool for mapping the spatial distribution of rich clusters. X-ray astronomy therefore offers a much improved identification method.

The *ROSAT* mission will have a strong impact on the study of clusters of galaxies. The *ROSAT* All-Sky Survey (RASS; Voges 1992), which took place between 1990 August and 1991 January using the X-ray Telescope (XRT), has revealed approximately 50 000 new X-ray sources, of which some 5–10 per cent are expected to be clusters. The survey data will extend, by about an order of magnitude, the size of the All-Sky X-ray flux-limited catalogue of clusters. The present flux-limited sample of ~ 50 clusters (Lahav et al. 1989; Edge et al. 1990), compiled from the previous all-sky surveys of *HEAO-1* (Piccinotti et al. 1982) and *Ariel-V* (McHardy et al. 1981; Warwick et al. 1981) and various pointed observations with the *Einstein* Observatory and *EXOSAT*, has already produced several significant results. Lahav et al. (1989) have measured the two-point correlation function of clusters, demonstrating that the correlation length is large (~ 20 Mpc). Edge et al. (1990) have discovered the presence of evolution in the X-ray luminosity function of clusters, wherein the largest, most luminous clusters are most numerous at the present epoch (see also Gioia et al. 1990). Edge, Stewart & Fabian (1992) have shown that cooling flows in clusters are common, being present in 70–90 per cent of the X-ray brightest clusters. The increased sample size and lower flux limit provided by the RASS will enable a more detailed examination of these phenomena and provide important constraints on large-scale structure and its formation.

The work described here is the first stage of an optical follow-up study to the survey, investigating the X-ray

brightest clusters with the primary aim of obtaining their redshifts. We have also made an investigation of optical line emission in the central galaxies of the clusters. This emission, often associated with extended, filamentary nebulae in nearby central cluster galaxies, is common in clusters with X-ray inferred cooling flows (Cowie et al. 1983; Heckman et al. 1989). We also re-examine the relationship between line emission and the presence of excess blue continuum light (Johnstone, Fabian & Nulsen 1987, hereafter JFN87; Romanishin 1988). A value for the Hubble constant of $H_0 = 50$ km s^{-1} Mpc^{-1} and a cosmological deceleration parameter $q_0 = 0$ have been used in all appropriate calculations.

2 OBSERVATIONS AND REDUCTION

2.1 Target selection

We have selected sources detected in the RASS with X-ray centroids within 5 arcmin of catalogued Abell and Zwicky cluster centres and with XRT count rates ≥ 0.2 count s^{-1} ($\sim 10^{-12}$ erg cm^{-2} s^{-1}). At the time of our observations, ~ 30 per cent of the survey data had been processed and our sample is selected from that preliminary data set. (The count rates obtained from the standard RASS analysis are approximate, being most uncertain for nearby and extended sources. However, for a large sample, the level of accuracy provided is easily sufficient for our target selection purposes.) A relatively small fraction (< 10 per cent) of the coincidences are random. This number can easily be estimated from the number of coincidences at larger offsets (e.g. 20–30 arcmin). The majority of the sources in the RASS are stars which are easily identified on inspection of optical survey plates and from their characteristically soft X-ray spectra. Other random coincidences are more difficult to identify before optical observations have been made. The expected 'contamination' is a few per cent after the removal of stars, i.e. one in a sample of 30 (see Section 3.1). A full statistical analysis of the cross-correlation of the RASS sources and the Abell catalogue will be presented by Ebeling et al. (in preparation).

We have determined cluster redshifts by spectroscopically measuring the redshift of the brightest galaxy on the Palomar E plates lying within 2 arcmin of the X-ray centroid (a reasonable estimate for the uncertainty in this position – see Ebeling et al., in preparation). Luminous clusters, such as those in our sample, generally have a single dominant galaxy at their X-ray, and therefore gravitational, centres. [In the flux-limited sample of Edge et al. (1990), over 75 per cent have their brightest galaxy within 2 arcmin of the X-ray centre.] These galaxies will hereafter be referred to as XCD galaxies. Of the remainder, most are 'Coma-type' binary clusters with two dominant elliptical galaxies in their cores. Since XCDs are situated at the centre of the cluster potential, it can be expected that their redshifts will be consistent with that of the cluster to within a few 100 km s^{-1}. There are cases where the central galaxy is not at rest with respect to the galaxy velocity mean (Zabludoff, Huchra & Geller 1990), but the discrepancy is never more than 500 km s^{-1}. [It is plausible that, even in these cases, the redshift of the central galaxy accurately measures that of the dominant cluster potential (e.g. Abell 1795, where the X-ray emission is strongly peaked on to an XCD galaxy with a peculiar velocity of ~ 400 km s^{-1} with respect to the galaxy velocity mean; Hill et al. 1988).] This level of accuracy is perfectly adequate for our analysis of the X-ray data.

XCD identification was made with the aid of the Automated Plate Measuring machine (APM) and a Photometric Data Systems plate analysis system in Cambridge. These were used to produce detailed 10×10 arcmin^2 optical maps of the region of the cluster core on to which the X-ray centroid was superimposed. The APM maps contain detailed spatial and magnitude information for each object in the field and hence, with accurate X-ray centres, identification of the XCD becomes relatively straightforward. In those few cases where no obvious dominant galaxy was found (e.g. Abell 1682, Abell 2219), we have measured the redshifts of several plausible candidates. Fig. 1 shows two examples of the APM finding charts used. The charts have each been centred on the *ROSAT* X-ray centroid. In both cases the XCD galaxy is easily identified as the dominant galaxy close to the centroid.

2.2 Observing strategy

The observations were made over the period 1991 June 4–10 with the Faint Object Spectrograph (FOS; Allington-Smith et al. 1989) on the 2.5-m Isaac Newton Telescope, La Palma. The FOS is a fixed-format spectrograph with a CCD detector and is specifically designed for low-resolution spectroscopy over a wide spectral range. A cross-dispersing prism is used to produce two spectral orders with a total wavelength coverage of 3500–10 500 Å. The dispersion is 10.7 Å pixel^{-1} in the first order (5000–10 500 Å) and 5.4 Å pixel^{-1} in the second (3500–5500 Å). The resolution in the spectral direction is 1.5 pixels.

Our observations were made with a 300-μm wide slit (corresponding to an image scale at the slit of ~ 1.6 arcsec), except in the case of flux standard stars, where the slit was opened to 1000 μm (~ 5.4 arcsec). The slit length was 6 arcsec. Standard stars were observed regularly throughout the night. Typical exposures on target galaxies were 1000 s. Observations were made at the parallactic angle to minimize the effects of atmospheric dispersion. Each target observation was immediately followed by an observation of a nearby F8 star, selected from an on-line catalogue, which was later used in the data reduction to remove atmospheric absorption from the spectra. Seeing was typically ~ 1.2 arcsec (FWHM). Flat-fields were generated using a tungsten lamp. Copper–argon arc exposures were taken for wavelength calibration.

A series of comparison observations using the Intermediate Dispersion Spectrograph (IDS) were also made. These observations were made using the 500-mm camera and a R400R grating, giving a dispersion of 1.10 Å pixel^{-1}. Again, a slit width of 300 μm was used.

2.3 Data reduction

The spectra have been reduced using the FOS Automated Reduction and Control Environment (FARCE). This software, which forms part of the ARK data reduction package and has been extended by us for the present project, automatically applies the following reduction algorithm to the spectra.

Raw frames are first debiased (using the chip overscan) and flat-fielded. The spectra are extracted from the frames

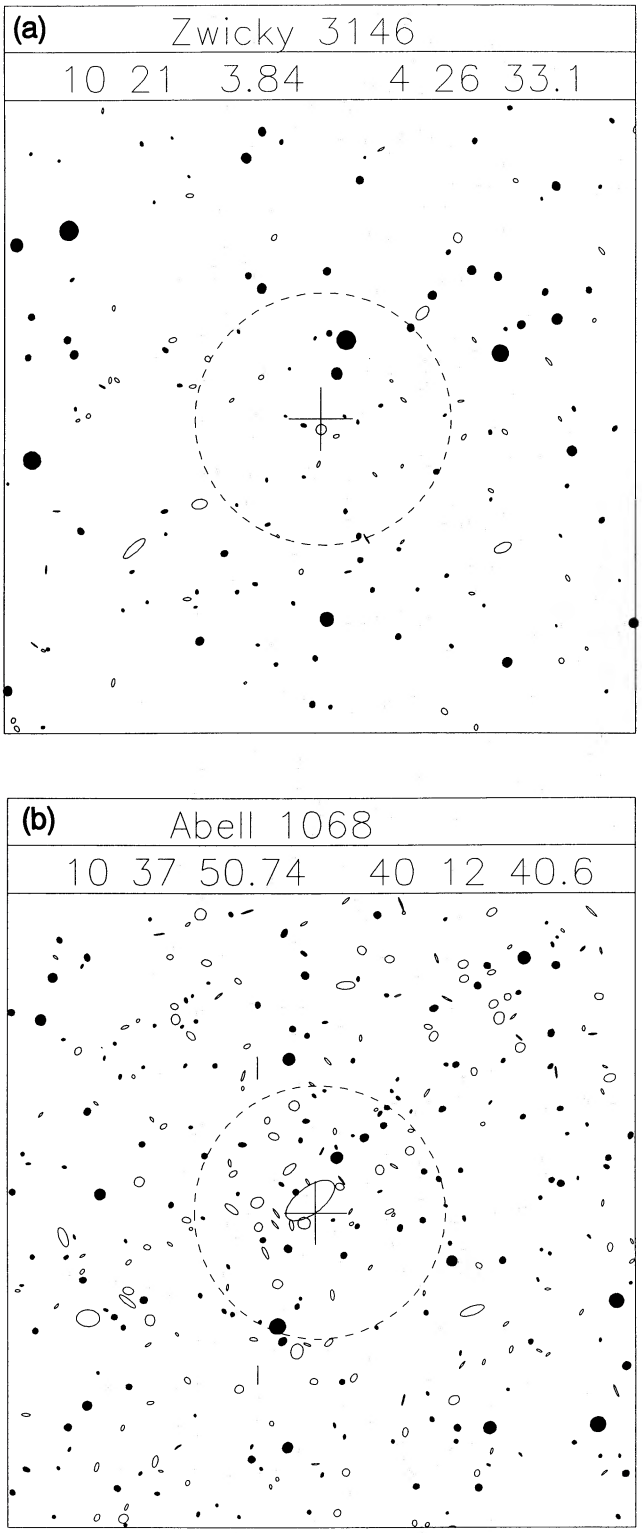

Figure 1. Examples of the APM machine finding charts used. The charts cover a region 10×10 arcmin^2 in size and are centred on the *ROSAT* XRT centroid, marked with a (1-arcmin diameter) cross. A 2-arcmin (radius) error box for the centroid is overlaid. The orientation has north to the top of the chart and east to the left. Filled circles correspond to stellar objects, open ellipses to galaxies or merged objects. The chart labels give the cluster name and X-ray centroid (1950 coordinates). The clusters shown are: (a) Zwicky 3146, the most distant new cluster observed at $z = 0.2906$; (b) Abell 1068 at $z = 0.1386$.

using the optimal extraction algorithm of Mukai (1990). Wavelength calibration is then applied. Atmospheric absorption features are removed using the exposures of F8 stars that accompany each target observation. F8 stars have particularly featureless continua in the 5000–10 500 Å wavelength region that forms the first spectral order, where atmospheric effects are most significant. FARCE fits a low-order polynomial to the F8 spectra and generates correction coefficients which are then used to correct the galaxy and standard star spectra for these effects.

Flux calibration used observations of the standard stars HZ44 and Wolf 1346. A default instrument response function (IRF), which describes the ratio of incident flux/observed counts as a function of wavelength for the FOS, was constructed from several photometric observations of these stars, with high signal-to-noise ratios. Standard stars were observed approximately hourly throughout the night so that galaxy observations would be accompanied by flux standard stars observed under approximately the same conditions. The individual standard observations were each used to produce an individual IRF from the observed distribution of counts and the known photometric, total fluxes. These were then fitted to the default IRF through multiplication by a low-order polynomial and the best-fitting results used to calibrate the fluxes of the associated galaxy spectra. In this way we have maintained an accurate and consistent flux calibration throughout.

The spectra have been corrected for reddening due to interstellar galactic extinction using the galactic hydrogen column densities of Stark et al. (1992). The transformation from $N(\mathrm{H\,I})$ to $E(B-V)$ was applied using the relation of Bohlin, Savage & Drake (1978):

$$\frac{N(\mathrm{H\,I})}{E(B-V)} = 4.8 \times 10^{21} \text{ atom cm}^{-2} \text{ mag}^{-1}.$$

The reddening law of Seaton (1979) and Howarth (1983) has been applied. Finally, the individual spectral orders from each observation are joined to form single spectra with complete wavelength coverage from 3500–10 500 Å.

The IDS spectra were reduced with the FIGARO data reduction package. F8 stellar spectra were again used to correct for atmospheric extinction.

2.4 Redshift determination

The redshifts were evaluated using the cross-correlation algorithm of Tonry & Davis (1979). The flux-calibrated spectra were rebinned into velocity space, with the scale such that a single bin corresponded to ~ 140 km s^{-1}. A fourth-order polynomial was fitted to and subtracted from the data to remove the continuum. Endmasking of 5 per cent was applied to each end of the spectra by multiplication with a cosine bell function. Two different templates were used in the correlation analysis. Absorption features in the spectra were cross-correlated against an observation of a K5 giant star with a particularly high signal-to-noise ratio. For this analysis, any strong emission lines in the galaxy spectra were removed and replaced with a linear interpolation across the continuum. Those spectra with emission features were also cross-correlated with an observation of the cD galaxy of Abell 1795. This galaxy has strong emission features with a

well-determined heliocentric redshift, $z = 0.0634$ (Hill et al. 1988) and is, therefore, well suited as a template for determining the redshift of the emission regions. It is important to recognize, however, that emission regions may have measurably different velocities (by ~ 100 km s^{-1}) from that of the underlying stellar continuum, and it is therefore sensible to determine both emission and absorption feature redshifts whenever possible.

For the correlation against absorption features, only those regions of the spectra between the Ca *H* λ3933 and Na *D* λ5892 features were used. For the emission-line redshifts, we selected those regions from [O II]λ3727 to [S II]λ6724. By using such selected wavelength regions, we were able to optimize the signal-to-noise ratio of the correlation function obtained.

The cross-correlation and redshift determination was performed using the FIGARO program SCROSS. The errors associated with our results were estimated using the prescription given in Tonry & Davis, i.e.

$$\varepsilon = \frac{PQ}{1+R},$$

where ε is the redshift error in km s^{-1}, P is bin width in km s^{-1} and Q the mean distance from the position of the largest peak in the correlation function to the nearest neighbouring peak. R is a factor determined for each correlation function, given by

$$R = \frac{H}{\sqrt{2}A},$$

where H is the height of the largest peak in the correlation function and A is the rms value for the height of a peak in the antisymmetric component of the correlation function.

3 RESULTS

3.1 Redshifts

From the original sample of 33 clusters meeting our selection criteria, we have obtained 28 XCD redshifts. One other cluster, Abell 1682, is an obvious binary candidate with two equally dominant elliptical galaxies, bringing the total of new cluster redshifts to 29. For the four remaining clusters, insufficient signal-to-noise ratios have prevented reliable redshift determinations and further spectra are required. Identification of the XCD in both Abell 2219 and 1703 was difficult and we have therefore measured the redshifts of all likely candidates in the respective fields. [Imaging work, performed by us on the Jacobus Kapteyn Telescope (JKT), La Palma, in 1992 January has since confirmed the XCD identifications. These are indicated in Table 1.] A full list of target observations and the determined absorption and

Table 1. New cluster redshifts.

Name	ROSAT ref.	RA(1950)	DEC(1950)	z(e)	err	z(a)	err	$W_{H\alpha}$(Å)
Z3146	RX J1023.7+0411	10 21 03.8	04 26 23	0.2906	0.0001	—	—	618±255
Z3179	RX J1025.9+1241	10 23 18.1	12 56 24	0.1434	0.0003	0.1432	0.0005	36 ±9
A1023	RX J1028.0−0648	10 25 28.3	−06 32 51	—	—	0.1165	0.0005	−1 ±2
A1033	RX J1031.7+3503	10 28 52.6	35 17 55	—	—	0.1259	0.0006	−2 ±3
A1045	RX J1035.0+3042	10 32 11.6	30 57 09	—	—	0.1381	0.0007	0 ±3
A1068	RX J1040.7+3957	10 37 51.3	40 12 51	0.1386	0.0001	—	—	309±122
A1084	RX J1044.5−0704	10 42 01.7	−06 48 23	0.1324	0.0005	0.1329	0.0007	22 ±4
A1204	RX J1113.4+1736	11 10 42.3	11 52 00	0.1706	0.0003	—	—	32 ±9
A1361	RX J1143.7+4622	11 41 00.2	46 37 59	0.1167	0.0002	0.1167	0.0005	70 ±16
Z4673	RX J1157.0+2415	11 54 21.5	24 32 18	—	—	0.1419	0.0006	2 ±2
A1664	RX J1303.8−2414	13 01 00.7	−23 58 37	0.1276	0.0002	—	—	264±43
A1672	RX J1304.4+3335	13 02 01.7	33 51 34	—	—	0.1882	0.0007	−7 ±3
A1682(1)	RX J1306.9+4633	13 04 32.1	46 49 31	—	—	0.2190	0.0004	0 ±2
A1682(2)	RX J1306.9+4633	13 04 36.3	46 49 33	—	—	0.2330	0.0004	3 ±2
A1703(1)	RX J1315.1+5149	13 12 58.6	52 04 52	—	—	0.2836	0.0003	−1 ±3
A1703(2)	RX J1315.1+5149	13 13 04.5	52 04 52	—	—	0.2336	0.0007	4 ±4
A1835	RX J1401.0+0253	13 58 30.0	03 07 10	0.2523	0.0001	0.2532	0.0008	147±40
A2104	RX J1540.1−0319	15 37 31.0	−03 08 38	—	—	0.1554	0.0008	−2 ±2
Z7707	RX J1555.0+1105	15 52 38.1	11 13 09	0.0401	0.0005	0.0413	0.0005	10 ±2
A2146	RX J1556.1+6622	15 55 51.8	66 29 32	0.2337	0.0002	0.2343	0.0006	217±87
Z7833	RX J1610.0+6711	16 09 47.9	67 17 56	—	—	0.2136	0.0004	1 ±3
A2208	RX J1629.8+5831	16 28 46.0	58 38 18	—	—	0.1329	0.0004	−5 ±2
A2219(2)	RX J1640.3+4642	16 38 45.8	46 48 27	—	—	0.2250	0.0007	−1 ±4
A2219(1)	RX J1640.3+4642	16 38 53.6	46 48 24	—	—	0.2248	0.0006	4 ±4
A2219(3)	RX J1640.3+4642	16 38 54.8	46 48 30	—	—	0.2344	0.0005	−2 ±2
A2228	RX J1648.0+2957	16 46 02.8	30 02 25	—	—	0.1013	0.0008	−3 ±2
Z8193	RX J1717.3+4227	17 15 45.3	42 30 06	0.1829	0.0001	0.1754	0.0006	56 ±10
A2318	RX J1905.7+7805	19 08 12.6	78 00 12	—	—	0.1405	0.0005	−4 ±2
Z8451	RX J1957.2+5751	19 56 13.7	57 43 15	—	—	0.0884	0.0001	−0.8 ± 0.2
Z8503	RX J2120.2+2258	21 20 04.1	22 57 39	—	—	0.1430	0.0006	−4 ±2
A2409	RX J2158.5+2043	21 58 31.6	20 43 41	—	—	0.1470	0.0007	−4 ±5
A2426	RX J2211.9−1037	22 11 52.2	−10 37 22	—	—	0.0990	0.0005	−1 ±1
A2428	RX J2213.6−0935	22 13 36.9	−09 34 58	—	—	0.0846	0.0005	1 ±1

Notes: (i) for A2219 and A1703, galaxy (1) is the most likely XCD; (ii) for A1682, (1) and (2) are equally dominant galaxies; (iii) for Z8451 the redshift and $W_{H\alpha}$ values are the mean of four separate spectra (see Table 2).

emission feature redshifts are given in Table 1. Heliocentric corrections have been applied to all values.

A control sample of clusters with known redshifts was observed to verify the reliability of our redshift evaluation. The results summarized in Table 2 show good, general agreement between our values and previous results. However, in one example, the XCD galaxy of Abell 1246 (Sandage, Kristian & Westphal 1976), there is a significant discrepancy between the two values. We cannot understand this difference, since the signal-to-noise ratio in our spectrum is excellent (see Fig. 2f).

The consistency of our redshift error-evaluation algorithm has also been examined. Four individual observations of the same cluster, Zwicky 8451, were made and redshifts derived for each. The results, also included in Table 2, are in excellent agreement and show consistent and reasonable errors.

Fig. 2 shows some examples of the fully reduced spectra with the two spectral orders merged together. An IDS spectrum of Abell 1068 has been included for comparison purposes (see Section 4).

The one clear candidate for possible contamination of our sample by X-ray sources other than clusters is Abell 2228. For this cluster the X-ray centroid is ~4 arcmin away from the most optically dominant galaxy, whereas it is only ~20 arcsec away from an optically bright active galactic nucleus (AGN). Both the AGN and optically dominant galaxy are members of the same cluster (their redshifts are separated by only ~1000 km s^{-1}) but, without a better X-ray image, we cannot be sure whether the AGN or cluster is the dominant X-ray source. As stated in Section 2.1, contamination at a level of a few (~3) per cent is what we would expect for the brightest cluster sample as a whole.

3.2 Emission lines

Emission-line nebulae are frequently found surrounding the central galaxy in clusters of galaxies with cooling flows (Cowie et al. 1983; Heckman et al. 1989). As gas cools from 10^6 to 10^4 K, its dominant cooling mechanism is optical and UV line emission. One might naively expect that the nebulae are simply formed from the cooling intracluster gas seen in X-ray observations, but the line luminosities observed are orders of magnitude greater than the level expected from simple recombination of the cooling gas (JFN87). The observed emission must be powered by another energy source. 'Simple' heating models such as photoionization by an active galactic nucleus, repressurizing shocks driven by the intracluster medium (ICM), ionization from massive stars formed from the cooling gas with a 'normal' initial mass function (IMF), and heating via X-rays from the ICM have all failed to satisfy the observational constraints (JFN87; Johnstone & Fabian 1988; Heckman et al. 1989). Although Donahue & Voit (1991) successfully reproduce the observed line ratios with an X-ray irradiation model, the very high X-ray fluxes needed are not observed and would require that the X-ray emitting gas is cooling on a time-scale faster than the gravitational free-fall time-scale, the maximum rate at which the gas could presumably be supplied. Recent work by Crawford & Fabian (1992) does, however, offer one plausible explanation for the observed line emission which evades these problems (see Section 4).

We have found clear evidence for optical line emission in 11 of the 28 XCD galaxies. (We define the presence of this emission to be the detection of the blended Hα+[N II] emission-line complex at a 5σ level.) In several cases the measured line luminosity is quite spectacular. Five of the galaxies provide Hα slit luminosities $\geq 10^{42}$ erg s^{-1}. The most extreme example, Zwicky 3146, has an Hα slit luminosity exceeding 8×10^{42} erg s^{-1}. As discussed above, the optical line emission is thought to be generated in extended filamentary regions surrounding the central galaxy in cooling flow clusters. The scale of this emission, typically ~2–5 kpc (or even larger in exceptional cases like NGC 1275), produces an image of comparable size to the slit width (1.5 arcsec) used for our observations. Hence, especially for those clusters at lower redshifts, our detections should be regarded as lower limits. The total Hα luminosity measured in imaging studies of NGC 1275, previously the most Hα-luminous XCD galaxy observed, is $\sim5\times10^{42}$ erg s^{-1} (Cowie et al. 1983). Clearly, however, several of our galaxies can be expected to possess similar total luminosities. Zwicky 3146 is the most extreme example of such emission at redshift ≤ 1.

Fig. 3 illustrates the clear differences between an optical spectrum of the central region of NGC 1275 (which contains a strong active nucleus) and that of Zwicky 3146, selected

Table 2. Control redshifts.

Name	ROSAT ref.	RA(1950)	DEC(1950)	z(e)	err	z(a)	err	z(published)
A1246	RX J1124.0+2129	11 21 21.0	21 45 15	—	—	0.1904	0.0006	(a) 0.216
A1651	RX J1259.4–0411	12 56 47.6	–03 55 36	—	—	0.0860	0.0004	(b) 0.0853±0.0002
Z5694	RX J1305.9+3054	13 03 30.1	31 10 04	—	—	0.1845	0.0006	(c) 0.1832
A1758	RX J1332.7+5033	13 30 38.7	50 49 01	—	—	0.2792	0.0005	(d) 0.280
1455+223	RX J1457.2+2220	14 55 00.5	22 32 31	0.2578	0.0003	—	—	(e) 0.258
A2187	RX J1624.2+4114	16 22 33.7	41 21 26	—	—	0.1839	0.0005	(f) 0.1830
Z8451(1)	RX J1957.2+5751	19 56 13.7	57 43 15.8	—	—	0.0884	0.0004	
Z8451(2)	RX J1957.2+5751	19 56 13.7	57 43 15.8	—	—	0.0887	0.0004	
Z8451(3)	RX J1957.2+5751	19 56 13.7	57 43 15.8	—	—	0.0885	0.0003	
Z8451(4)	RX J1957.2+5751	19 56 13.7	57 43 15.8	—	—	0.0885	0.0004	

Refrences: (a) Sandage, Kristian & Westphal (1976); (b) Zabludoff, Huchra & Geller (1990); (c) Abell, Corwin & Olowin (1989); (d) Mason et al. (1981); (e) Kristian, Sandage & Westphal (1978); (f) Ciardullo et al. (1983).

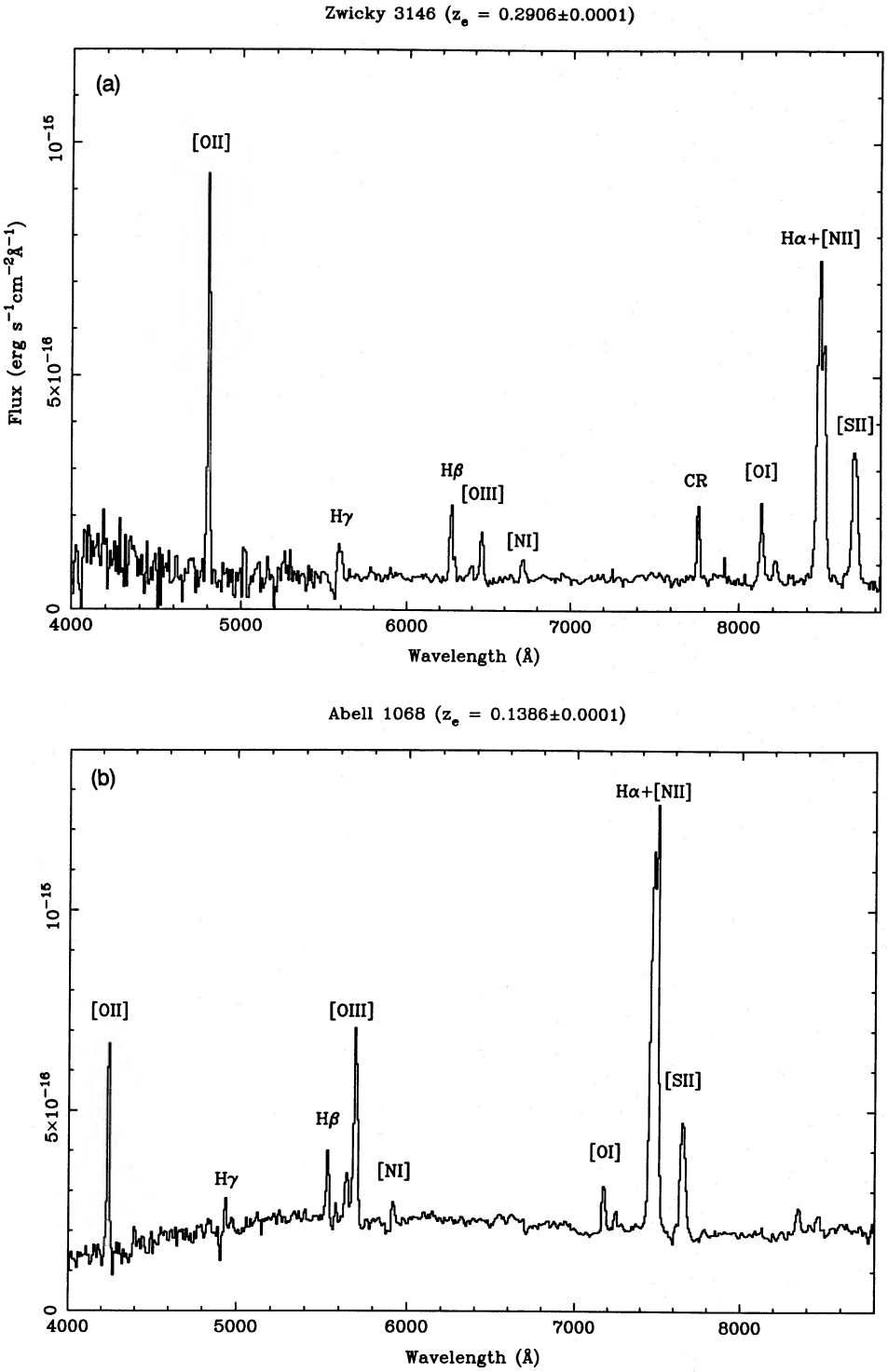

Figure 2. A selection of the XCD galaxy spectra obtained. (a) Zwicky 3146, (b) Abell 1068, (c) Abell 1835, (d) Abell 2146, (e) Zwicky 7833, (f) Abell 1246, the XCD for which our redshift value differs from the published value, all obtained using the FOS. (g) IDS spectrum of Abell 1068.

from our sample. Both objects have comparable overall Hα luminosities (the slit luminosity for the NGC 1275 observation is $\sim 2\times10^{42}$ erg s^{-1} at a redshift of 0.0183) but very different velocity widths. NGC 1275 has a (FWHM) Hα velocity width $\sim$3500 km s^{-1}, with some evidence for an even broader underlying component. In contrast, the velocity width of Zwicky 3146 is only $\sim$600 km s^{-1}, a value representative for our whole sample (see Table 3).

The distribution of the observed equivalent widths of the Hα + [N II] line complex is shown in Fig. 4. The values have been calculated by fitting a combination of a single Gaussian line and a linear continuum to each spectrum in the relevant

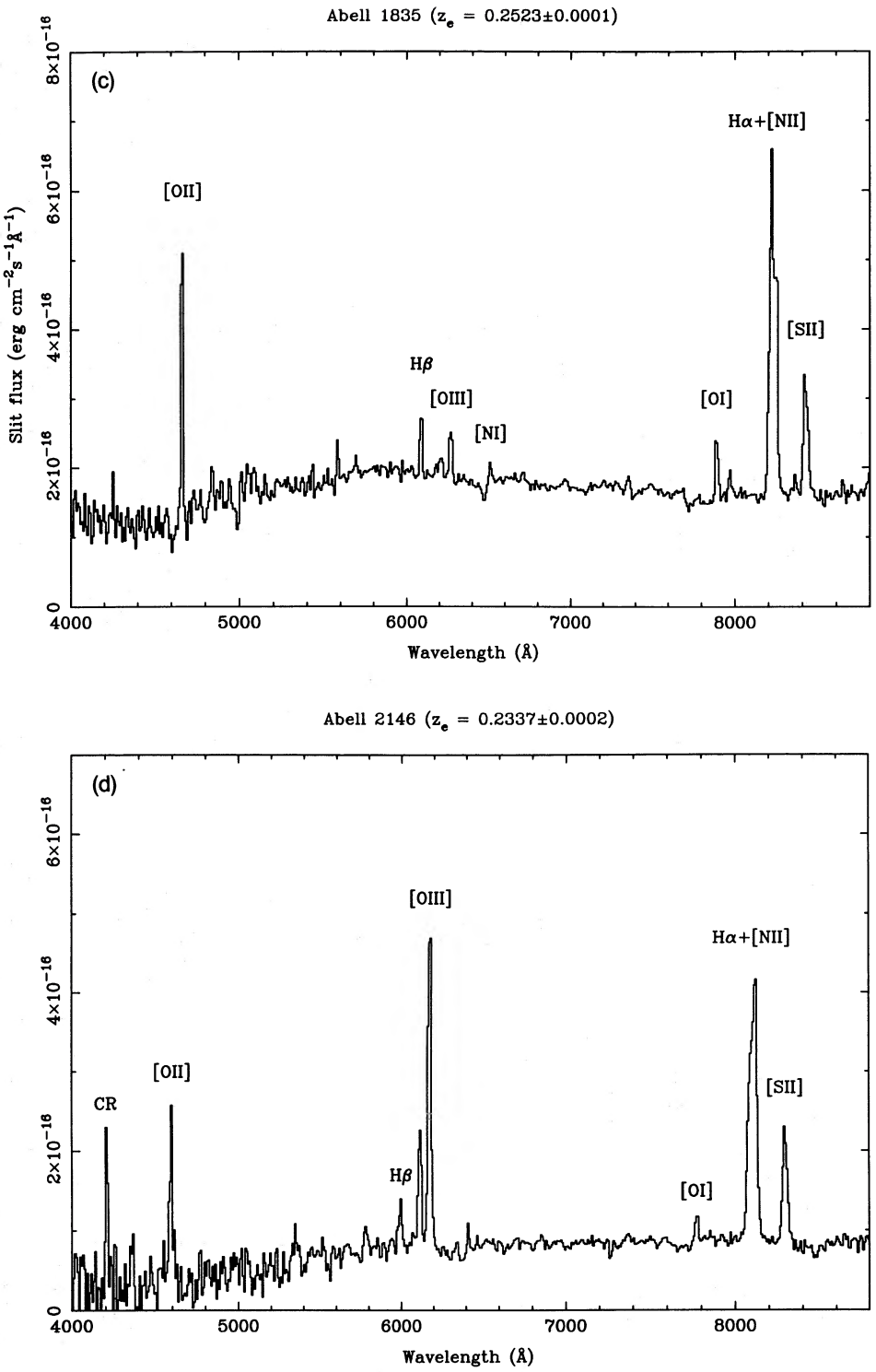

Figure 2 – *continued*

wavelength regions. For those clusters with no obvious emission we have calculated limits by fixing a suitable Gaussian width (the mean of the values in the positive detections), evaluating the central position from the redshifts and then refitting the model. The figure shows that there is no steady decrease in the number of observed galaxies as we move to higher equivalent widths. We note that those galaxies for which $W_{H\alpha+[N\,II]} \leq 0.1$ Å have been counted in the left-most bar of the histogram.

The fluxes in the most prominent emission lines have been measured and are summarized in Table 3. Ratios of the line fluxes have been calculated and used to construct the line ratio diagrams plotted in Fig. 5. The individual fluxes in the blended Hα λ6563 and [N II] $\lambda\lambda$6548, 6583 lines have been

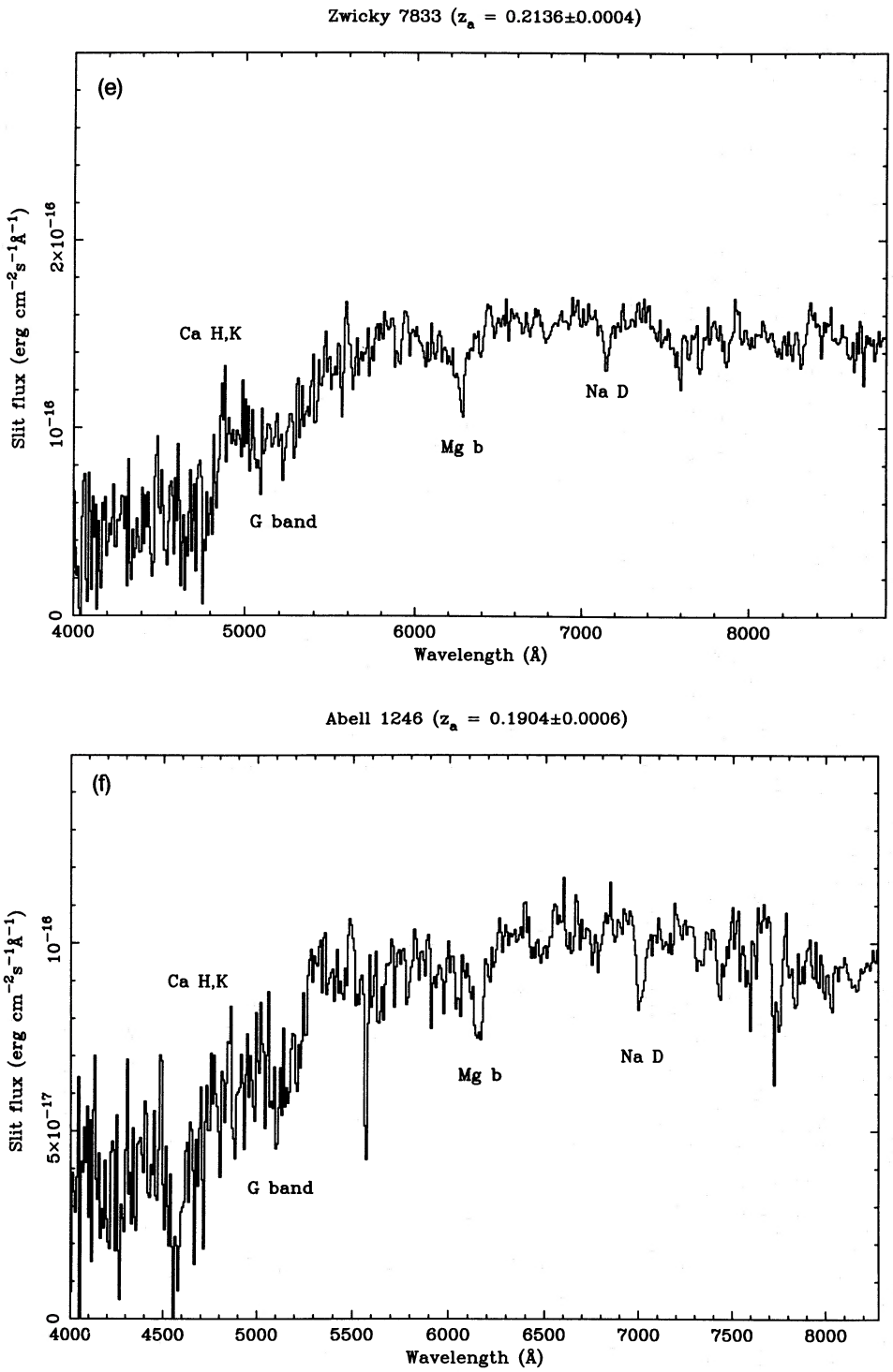

Figure 2 – *continued*

obtained by fitting a triple Gaussian model to this complex, in which all three lines are forced to have the same redshift and velocity width, and the relative normalization of the [N II] $\lambda\lambda$6583 and 6548 lines is fixed at the appropriate value of 3/1. The flux quoted for the [S II] line is the total in the blended $\lambda\lambda$6716, 6731 doublet.

Several trends are clearly visible in the line ratio diagrams. Where measurable, the [O II]/[O III], [O III]/Hβ and [N II]/Hα ratios can be used to split the galaxies into two subsets, class I and class II (Heckman et al. 1989). The class II XCDs (e.g. Abell 1835, Abell 1664 and Zwicky 3146) all have strong Balmer/forbidden-line ratios and high [O II]/[O III]. The class I XCDs (e.g. Abell 2146 and 1068) have much weaker Balmer/forbidden-line ratios and a smaller [O II]/[O III] ratio, indicative of significantly higher states of ionization. Other line ratios constructed from Table 3 were examined but did

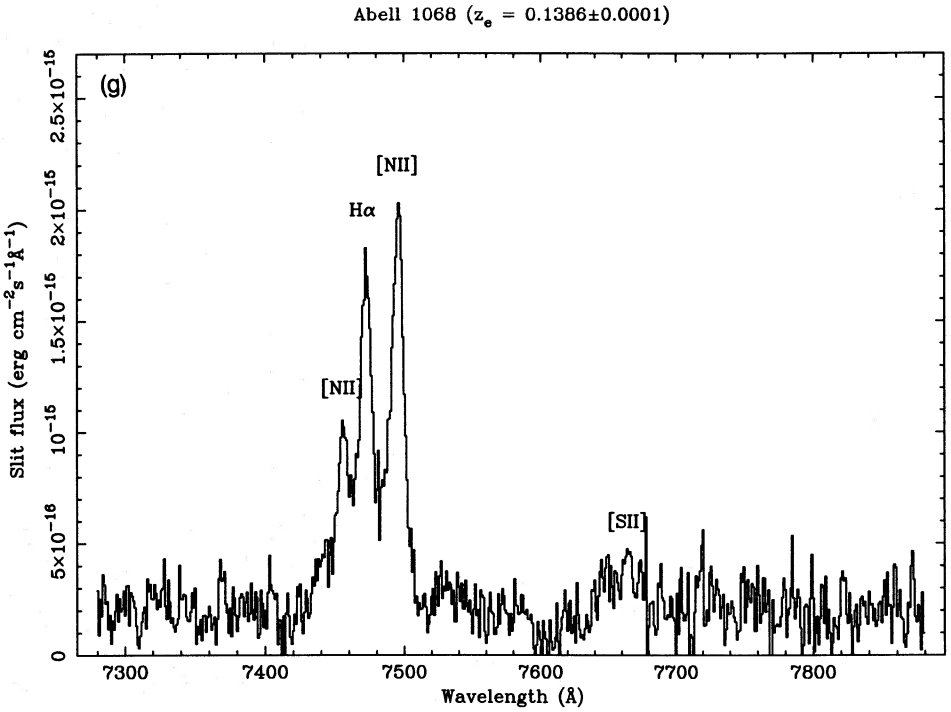

Figure 2 – *continued*

not demonstrate any clear class separations. In contrast to the study of Heckman et al. (1989), we find no clear distinction between the two classes in terms of either their X-ray or Hα luminosities (see Tables 4 and 5). Both Abell 1068 and 2146 are examples of high-luminosity class I systems. Also, rather than providing a clear split into two classes, the line ratios generally seem to show a more continuous distribution (see also Crawford & Fabian 1992). No clear correlation between the FWHM Hα velocity width and other measured properties of the emission lines exists.

The line fluxes and velocity widths derived from the IDS spectra of Abell 1835, 1068 and 2146 are summarized in Table 6. The IDS values show excellent agreement with those obtained from the FOS spectra.

3.3 Excess blue light

Several previous studies (e.g. JFN87; Romanishin 1988; McNamara & O'Connell 1989) of XCD galaxies in cooling-flow clusters have noted the presence of an excess of blue continuum light, over and above that associated with a normal old elliptical galaxy. This excess is generally thought to be emission from a population of hot, young stars in the central region of the galaxy. Certainly, at least some such stars are required to explain the A-star optical spectral features of NGC 1275, the central galaxy of the Perseus cluster (Rubin et al. 1977), and the F-star absorption features associated with the XCD in Abell 1795 (McNamara & O'Connell 1989).

The sample spectra in Fig. 2 demonstrate a clear difference between the continuum shapes of XCD galaxies with emission lines and those without. Emission-line XCDs generally have much bluer continua, with little (if any) decrease in flux towards shorter wavelengths. We have fitted each of the emission-line spectra with a model consisting of an elliptical galaxy template (we used the spectrum of Zwicky 7833 for this purpose) and a component due to emission from young, massive stars. The young stellar component has been modelled by a single spectrum of a massive star, generated from the models by Kurucz (1979). (The most massive stars will dominate a blue stellar continuum formed with any 'reasonable' initial mass function.) The fits have been performed in the rest frame of the galaxies, over wavelengths ranging from the bluest available (~ 3000 Å for most of the galaxies) out to 6250 Å (beyond which emission-line features tend to dominate the spectra). In each case, we find that surprisingly good fits to the XCD galaxy continuum can be obtained with an additional stellar component consistent with emission from B stars (see Fig. 6). The results, summarized in Table 4, indicate that for most galaxies the best fits were obtained using a reasonable number (10^6–10^8) of B5 main-sequence stars with an effective temperature $T_e \approx 16\,000$ K. However, for Zwicky 3146, the most line-luminous XCD galaxy, a much better fit was obtained using a stellar component dominated by B0 stars ($T_e \approx 30\,000$ K). Other models, where the excess blue light was fitted with a power-law component, were tested but did not produce such good fits to the data. The blue continuum must either be due to massive B stars or to some process which emits a continuum very similar to that of B stars over the wavelength interval 3000–6000 Å.

To quantify the amount of excess blue light present in the spectra, we have defined the quantity δBR, where

$$\delta BR = \frac{\int_{3500}^{3650} F_\lambda \delta\lambda}{\int_{5800}^{6200} F_\lambda \delta\lambda}.$$

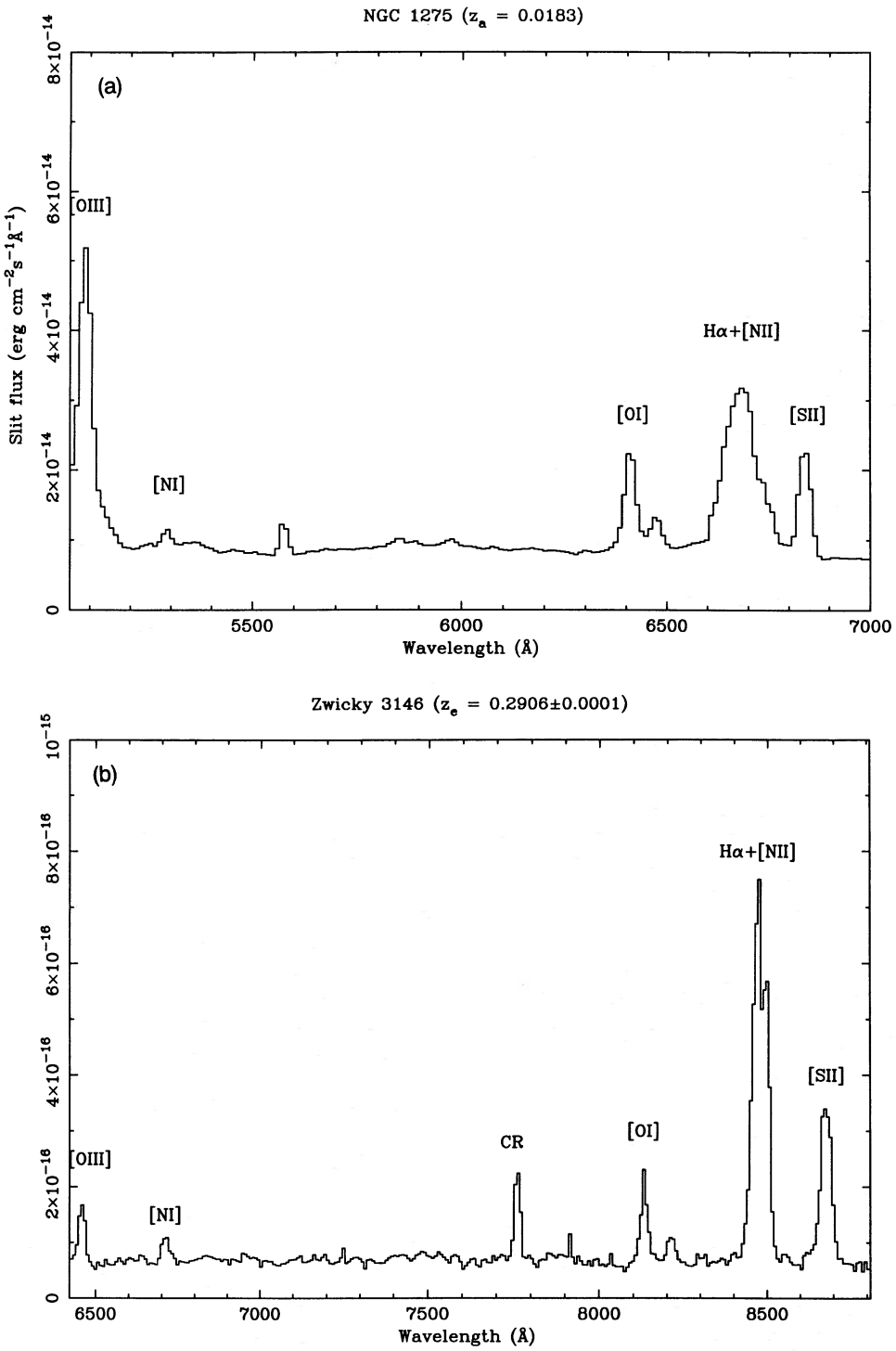

Figure 3. (a) FOS spectrum of NGC 1275 (taken from Johnstone & Fabian 1988). (b) 1991 June FOS spectrum of Zwicky 3146 illustrating differences in the spectral features when compared to NGC 1275.

The limits on the integrals correspond to wavelengths in the galaxy rest frames. The values were chosen to use the blue-most flux present in the spectra (where the contribution to the observed flux from the underlying elliptical galaxy is least significant) and to avoid any strong emission-line features. Table 4 lists the calculated values of δBR. Fig. 7 shows how δBR varies with the measured Hα luminosity and [N II]/Hα ratio.

3.4 X-ray data

The X-ray properties of the five most optically line-luminous clusters are summarized in Table 5. Fluxes have been calculated for count rates measured in the central 1 Mpc (radius) region of the clusters. A model, consisting of emission from a hot, isothermal, diffuse plasma (Raymond & Smith 1977) of temperature 5 keV and metallicity 0.4 solar,

with photoelectric absorption from the appropriate galactic column densities (Stark et al. 1992) has been used in converting count rates to actual fluxes in the 0.1–2.4 keV XRT bandpass. A simple extrapolation of the model has been applied to calculate the predicted 2–10 keV fluxes quoted in column 4 of Table 5, thus enabling a direct comparison with the list of the 50 X-ray brightest clusters (Lahav et al. 1989; Edge et al. 1990) to be made.

The short (~ 500 s) exposures in the XRT Survey make a detailed analysis of the X-ray properties of the individual clusters difficult, although the exposures were long enough to allow us to determine the central cooling time within radii of 150–300 kpc for each of the five clusters for which the original photon data were available. All of these show cooling times less than the Hubble time or very close to it once the effects of resolution are taken into account (Edge et al. 1992), and so can be classified as cooling flows. All of the remaining clusters have X-ray fluxes $\sim 2\text{–}5 \times 10^{-12}$ erg cm^{-2} s^{-1}, with the precise values depending on the spatial extent of the X-ray emission. These values will be reported in future work.

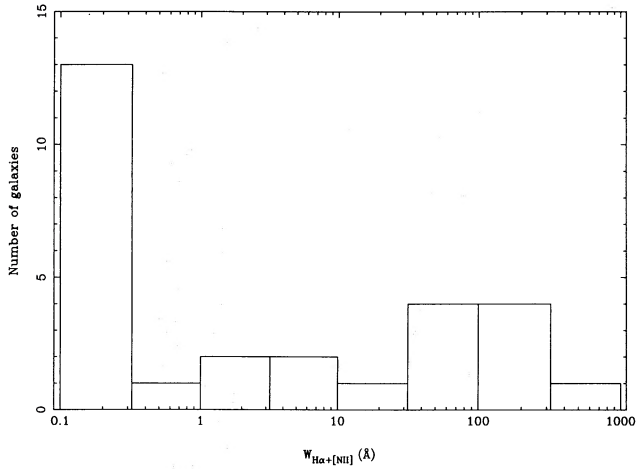

Figure 4. Distribution of the observed equivalent widths of the Hα + [N II] line complex. Galaxies with $W_{H\alpha+[NII]} \leq 0.1$ Å have been included in the left-most column.

3.5 Other wavelengths

We have cross-correlated our emission-line XCD galaxies with available radio surveys (e.g. Condon 5-GHz, Texas 365-MHz, Cambridge) and find that our galaxies are not generally associated with strong radio sources. [Two of the

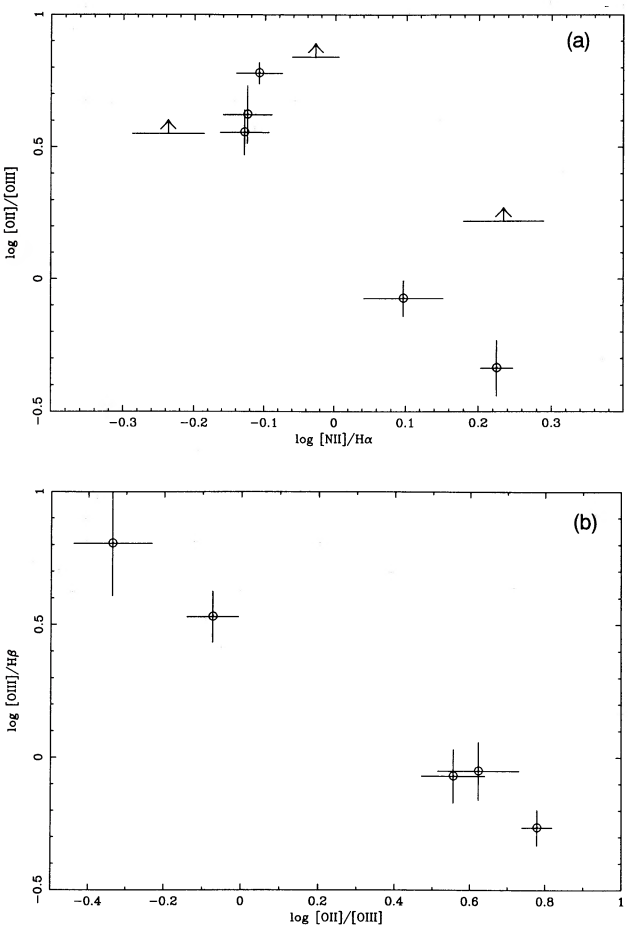

Figure 5. Line ratio diagrams demonstrating the Heckman et al. (1989) class separation: (a) [O II]λ3727/[O III]λ5007 versus [N II]λ6584/Hα λ6563; (b) [O III]λ5007/Hβ λ4861 versus [O II]λ3727/[O III]λ5007. Arrows indicate lower limits.

Table 3. Line fluxes.

Name	Hα λ6563	Hβ λ4861	[NII] λ6584	[NI] λ5199	[SII] $\lambda\lambda$6716,6731	[OIII] λ5007	[OII] λ3727	[OI] λ6300	Hα velocity width (FWHM km s^{-1})
A1835	105±5	20±3	78±5	5.2±2.5	57±8	17±3	61±5	21±3	460±60
A1068	189±17	34±6	236±21	10±3	106±7	115±15	97±8	29±3	540±130
Z3146	172±8	46±6	134±8	11±2	127±13	25±2	150±7	39±6	570±60
A2146	53±2	16±7	89±3	≤10	49±3	102±11	47±10	9±2	720±50
A1664	112±6	18±3	84±5	≤13	84±2	16±3	67±11	17±4	920±90
Z3179	9±3	≤2	28±5	≤4	19±6	≤9	≤11	10±3	770±210
Z8193	107±7	≤32	62±6	≤10	67±8	≤22	88±10	≤19	470±100
A1361	21±2	≤8	36±3	≤5	24±3	≤16	34±8	≤5	500±130
A1795	95±5	≤24	89±5	≤13	85±4	≤13	106±14	36±11	570±100

Notes: All fluxes in units of 10^{-16} erg s^{-1} cm^{-2}; error bars and upper limits are quoted at 90 per cent confidence level.

Table 4. Blue continuum components.

Name	F_{star}/F_{gal} (4500 Å)	F_{star}/F_{gal} (3500 Å)	δBR	N_{stars}	Predicted $L_{H\alpha}$	Measured $L_{H\alpha}$
A1835	0.34	0.76	0.28	7.7×10^{7}	3.1×10^{43}	$3.7\pm0.2\times10^{42}$
A1068	0.26	0.68	0.24	1.9×10^{7}	7.5×10^{42}	$1.8\pm0.2\times10^{42}$
Z3146	0.45	0.89	0.40	$*4.0\times10^{6}$	6.1×10^{43}	$8.2\pm0.4\times10^{42}$
A2146	0.16	0.52	0.14	1.0×10^{7}	3.9×10^{42}	$1.6\pm0.1\times10^{42}$
A1664	0.30	0.72	0.30	1.4×10^{7}	5.6×10^{42}	$8.9\pm0.5\times10^{41}$
Z3179	—	—	0.08	—	—	$9\pm3\times10^{40}$
Z8193	0.16	0.53	0.19	3.3×10^{7}	1.3×10^{43}	$1.8\pm0.1\times10^{42}$
A1361	0.05	0.22	0.11	1.0×10^{6}	3.9×10^{41}	$1.4\pm0.1\times10^{41}$
A1795	0.18	0.56	0.17	2.8×10^{6}	1.1×10^{42}	$1.8\pm0.1\times10^{41}$

Notes: predicted Hα fluxes are calculated using equation (5.24) from Osterbrock (1989); all fitted values are derived using Zwicky 7833 as an elliptical galaxy template; additional stellar components are modelled as a single B5 main-sequence stellar spectrum (* except Zwicky 3146 which is best fitted by a B0 spectrum), generated from the models of Kurucz (1979).

Table 5. X-ray data summary.

Name	F_X(0.1-2.4 keV) erg cm^{-2}s^{-1}	L_X(0.1-2.4 keV) erg s^{-1}	F_X(2-10 keV) erg cm^{-2}s^{-1}	L_X(2-10 keV) erg s^{-1}
A1835	7.9×10^{-12}	2.7×10^{45}	6.0×10^{-12}	2.1×10^{45}
A1068	8.2×10^{-12}	7.8×10^{44}	6.7×10^{-12}	6.3×10^{44}
Z3146	5.0×10^{-12}	2.4×10^{45}	3.7×10^{-12}	1.8×10^{45}
A2146	2.8×10^{-12}	8.1×10^{44}	2.1×10^{-12}	6.3×10^{44}
A1664	5.1×10^{-12}	4.1×10^{44}	4.3×10^{-12}	3.4×10^{44}

Note: all values derived with a model consisting of Raymond–Smith emission ($T=5$ keV, $Z=0.4$ $Z_\odot$) and galactic photoelectric absorption.

XCDs do contain significant sources, however; Abell 1361 has a 151-MHz flux density of 5.80 Jy (7C catalogue; McGilchrist et al. 1990) and Zwicky 8193 has a 4.85-GHz flux density of 134 ± 16 mJy (Gregory & Condon 1991, the detection limit of this catalogue being $S\geq25$ mJy).] Since many AGN at the centres of clusters are radio loud, this evidence suggests that photoionization by an active nucleus or other activity associated with the radio emission is unlikely to be the principal mechanism for generating the line emission.

Two galaxies in our sample are included in the *IRAS* Faint Source Catalog (Moshir et al. 1989). The XCDs of Abell 1068 (IRAS F10378+4012) and Abell 2228 (IRAS F16460+3003) have 60-μm flux densities of $S=575$ and 162 mJy respectively (NASA/IPAC Extragalactic Database).

4 DISCUSSION

We have presented redshifts for the XCD galaxy in 29 of the X-ray brightest clusters observed in the *ROSAT* All-Sky

Table 6. Summary of IDS observations.

Name	$F_{H\alpha}$ λ6563	$F_{[NII]}$ λ6584	Hα velocity width FWHM (km s^{-1})
A1835	94±12	69±11	380±50
A1068	188±8	225±10	510±20
A2146	50±7	81±7	650±50

Note: all fluxes in units of 10^{-16} erg s^{-1} cm^{-2}.

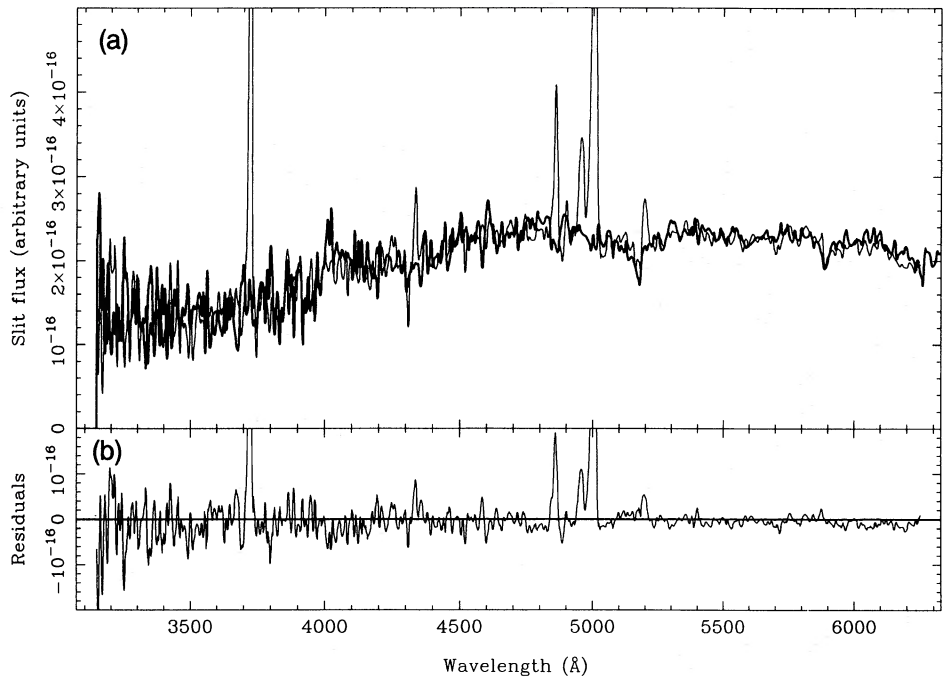

Figure 6. (a) The XCD of Abell 1068 (shifted to its rest frame) with the best-fitting model of an elliptical galaxy template (Zwicky 7833) and a B5 stellar component (Kurucz 1979) superimposed (the model is plotted as a thick line). (b) Residuals after subtracting the best-fitting model.

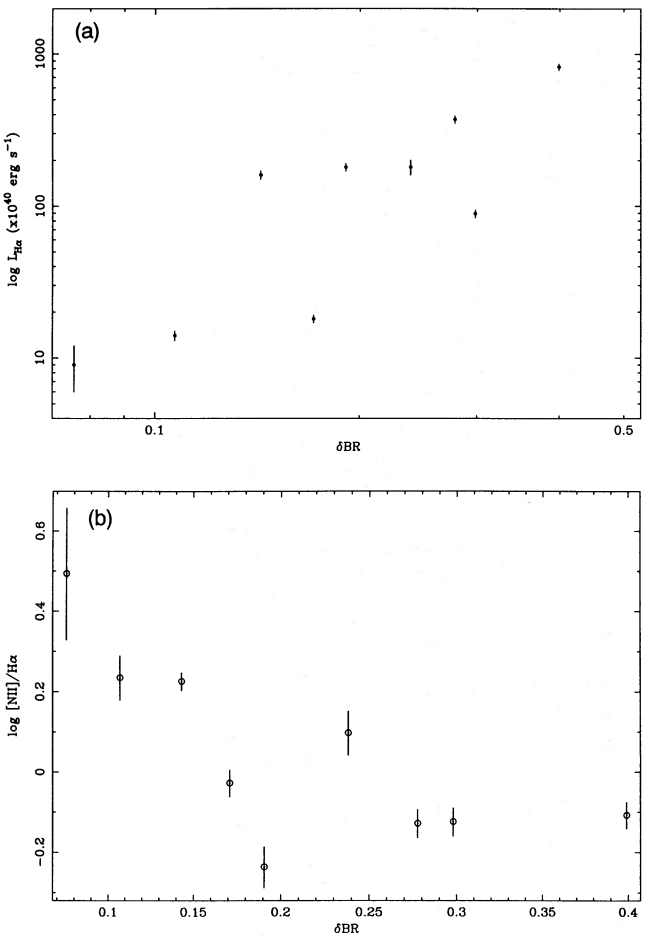

Figure 7. (a) Variation in the measured Hα luminosity with δBR. (b) Variation in the [N II]/Hα ratio with δBR.

Survey. We find that ~1/3 of the 3500–10 500 Å spectra show strong line emission. Where available, the X-ray data suggest that the emission-line clusters contain cooling flows. We have found that our emission-line XCD spectra are generally much bluer than those of standard XCD galaxies, and that the spectral shape of the excess blue continuum light is well matched to B stars. This suggests a link between line emission and the presence of a population of young ionizing stars, in addition to the generally late-type stellar population of such galaxies. We note, however, that vacuum ultraviolet spectra are required to discriminate further on the B-star model for the excess blue continuum flux.

The fate of the cooled matter in cooling flows has been a subject of active research. Early explanations examined the formation of large quantities of low-mass stars as a suitable end-point for the cooled matter. The recent discovery of large amounts of cold, absorbing gas in a sample of ~20 clusters by White et al. (1991), using *Einstein* SSS data, provides an alternative end-point, where much of the cooled matter simply remains as cold gaseous blobs, distributed about the base of the cluster potential. Nevertheless, the physical conditions within cooling flows should lead to at least some star formation, most probably with an IMF biased towards lower mass stars (see discussion in Fabian, Nulsen & Canizares 1991). Strong evidence for star formation has been found in the spectrum of NGC 1275, the XCD galaxy in the Perseus cluster (Abell 426). Perseus is the nearest large cooling-flow cluster ($z = 0.0183$) and shows a similar spectral shape to the bright emission-line galaxies in our sample (Kent & Sargent 1979), although (as shown in Section 3.2) the presence of a powerful, active galactic nucleus leads to significant line broadening in its centre. Recent work using the *Hubble Space Telescope* (Holtzman et al. 1992) has revealed the presence of a population of blue, point-like sources concentrated within 2–3 kpc of the galaxy centre, overlying the normal late-type elliptical population. Most are found to be continuum rather than emission-line sources, with scalesizes and colours consistent with massive star clusters.

Neither Perseus nor our sample of emission-line XCDs demonstrates the strong UV spectral up-turn generally associated with the presence of O stars. The B-star spectrum of the excess blue continuum is more suggestive of either continuous star formation with an IMF truncated at 10–20 $M_\odot$ or a recent starburst, spectrally dominated by B stars. The sizes of the observed young stellar components (Table 4) imply star formation rates of 0.2–20 $M_\odot$ yr^{-1} in B stars alone and total star formation rates (with a truncated 'normal' IMF) of between 0.5 and 100 $M_\odot$ yr^{-1}.

B stars can produce significant ionization in gas which surrounds them. Assuming that all of the ionizing photons emitted by such stars are absorbed in surrounding gas (i.e. the covering fraction of the gas is very high), and using the appropriate recombination coefficients from Osterbrock (1989), we find that the observed young stellar populations in our galaxies provide enough UV photons to account for the observed Hα emission (see Table 4).

From Section 3.3 we also see that a clear correlation exists between δBR and $L_{H\alpha}$, in agreement with results found by JFN87 for lower redshift XCD galaxies. Marginal correlations are observed with the [N II] and [O I] lines. XCDs with high Hα/[N II] ratios tend to have large δBR values (Fig. 7b). The evidence suggests that the Hα emission-line luminosity is related to the excess blue continuum flux. However, whether δBR and $L_{H\alpha}$ are directly correlated (i.e. whether a direct causal relationship exists between the two) is not clear; it may be that they both result from some other process.

Although stars alone can satisfy the energetic constraints on the observed line emission, they cannot reproduce the observed line ratios. H II regions generally occupy regions of the line ratio diagrams separate from those of XCD emission-line galaxies (e.g. see Robinson et al. 1987). In particular, normal main-sequence stars cannot reproduce the observed [N II]/Hα and [O III]/[O II]/[O I] ratios. A much harder UV spectrum than that generated by OB stars is required. (This is a problem for the interpretation of the excess blue light as being due to young stars alone, and may indicate that it has a more complex origin.) Since emission-line nebulosity in XCD galaxies has only been observed in cooling-flow clusters, we also require that the generation of emission lines should somehow be related to the presence of a cooling flow. The most plausible explanation to date (Crawford & Fabian 1992) involves a combination of the self-absorbed irradiation of small, cold gas clouds in mixing layers on the surfaces of large, cold molecular clouds, and emission from shocks generated in collisions between these clouds. The large amounts of cold gas in the cluster centre

required by this mechanism (and observed in the X-ray observations by White et al. 1991) will presumably have accumulated from the long-term deposition of material by a cluster cooling flow.

Since we do not spatially resolve our emission-line nebulosity, some level of ionization from an active nucleus remains possible. Nevertheless, the fact that we see no evidence for any broad (velocity width ≥ 1000 km s^{-1}) Seyfert-like emission lines in our spectra, and that our galaxies are not generally radio loud, and considerations of ionization equilibrium outlined by Johnstone & Fabian (1988) and Heckman et al. (1989), all suggest that photoionization by an active nucleus cannot be the dominant ionization mechanism in emission-line XCDs.

It is important to note that not all clusters in which there is X-ray evidence for a cooling flow exhibit optical line emission (nearby examples of this include Abell 2029 and 478). Only 11 of our sample of 29 (38 per cent) show significant optical line emission. This is consistent with the recent study by Edge, Stewart & Fabian (1992) indicating that 70–90 per cent of the 50 X-ray brightest clusters contain cooling flows but only 40 per cent show line emission. Therefore our sample is consistent with a high fraction of cooling flows (as predicted by Pesce et al. 1990) and the ratio of clusters showing line emission within $z = 0.1$ is similar to that for clusters of $z = 0.1$–0.25 (see also Donahue et al. 1992).

Nearly 20 per cent (five out of 29) of the XCD galaxies in our sample have $L_{\mathrm{H}\alpha} > 10^{42}$ erg s^{-1}. The efficiency with which most mechanisms produce Hα photons is $\lesssim 2$ per cent, implying that a source of $> 5 \times 10^{43}$ erg s^{-1} must be powering the observed emission in these clusters. The most likely source of this power is the thermal and kinetic energy of the surrounding intracluster gas.

Daines, Fabian & Thomas (1992) have used constraints from X-ray and 21-cm observations to show that the central (~ 10 kpc) regions of cooling flow clusters contain large masses ($\gtrsim 10^{10}$ M$_\odot$) of cold gas, in the form of small ($\ll 1$ pc) molecular clouds, in addition to a similar or greater mass of hot ($T \sim 2 \times 10^7$ K) gas. Cluster–subcluster mergers, such as those thought to cause the X-ray evolution of clusters, can lead to the deposition of large quantities of cold and cooling gas into the centre of the cluster (and to a merger of the cluster and subcluster central galaxies themselves), without causing serious disruption to the large-scale cooling flow (Fabian & Daines 1991). Such mergers also inject large amounts of kinetic energy into the cluster centres which then dissipates through cloud–cloud collisions. The increase in turbulence acts as a catalyst and increases the rate of mixing between the hot ICM and the cold gas by generating mixing layers on the surfaces of the clouds (Crawford & Fabian 1992). These cause much of the thermal energy of the hot gas to be channelled into optical and UV line emission (Daines et al. 1992). The maximum power, P_{max}, which can be channelled into optical line emission by this process is given by

$$P_{\mathrm{max}} \sim \frac{5 M_{\mathrm{H}} c_{\mathrm{s}}^3}{2l},$$

where M_{H} is the mass of hot gas in the region, c_{s} is the sound speed of the hot gas and l is the length-scale over which the emission is observed to occur coherently. On the assumptions $M_{\mathrm{H}} \sim 5 \times 10^{10}$ M$_\odot$, $c_{\mathrm{s}} \sim 400$ km s^{-1}, $l \sim 10$ kpc and a 2 per cent conversion efficiency for this power into Hα emission, this implies a maximum observable Hα luminosity of $L_{\mathrm{H}\alpha} \sim 10^{43}$ erg s^{-1}. Clearly, if such emission mechanisms are responsible for the observed line luminosities, objects like Zwicky 3146 with $L_{\mathrm{H}\alpha} \sim 10^{43}$ erg s^{-1} must be extreme examples. Such large luminosities also demand that the emission be transient, lasting for only a few dynamical times of $\sim 10^8$ yr, much less than the cluster-merger time-scale inferred by Edge et al. (1990). The presence of strong $L_{\mathrm{H}\alpha} \sim 10^{43}$ erg s^{-1}) optical line emission may therefore be one signature of a recent cluster merger and may enable the large optical follow-up study of the RASS X-ray brightest clusters to place further constraints on the nature of cluster evolution.

ACKNOWLEDGMENTS

The authors thank the *ROSAT* operations and analysis teams at MPE and GSOC for the smooth running and analysis of the survey and Professor Trümper for hospitality during many visits to MPE. The Isaac Newton Group of Telescopes at the Observatorio del Roque de los Muchachos del Instituto de Astrofisica de Canaris is operated by the Royal Greenwich Observatory on behalf of the Science and Engineering Research Council (UK) and the Nederlandse organisatie voor wetenschappelijk onderzoek (NL). The NASA/IPAC Extragalactic Database is operated by the Jet Propulsion Laboratory, California Institute of Technology (USA), under contract with NASA. We thank John Pilkington, Richard McMahon and Mike Irwin for their help in producing finding charts, and Paul Alexander and Stephen Hancock for their assistance in the cross-referencing of radio survey data. Thanks go to Chris Jomaron for his part in the development of the FARCE software. Finally, the authors thank Stuart Daines, Dave White and Paul Francis for interesting and stimulating discussions. SWA acknowledges receipt of a SERC studentship. ACE, CSC, RMJ and TN thank the SERC for support at MPE and Cambridge. ACF thanks the Royal Society for financial support.

REFERENCES

Abell, G. O., 1958. *Astrophys. J. Suppl.*, **3,** 211.
Abell, G. O., Corwin, H. G. & Olowin, R. P., 1989. *Astrophys. J. Suppl.*, **70,** 1.
Allington-Smith *et al.*, 1990. *Mon. Not. R. astr. Soc.*, **238,** 603.
Bohlin, R. C., Savage, B. D. & Drake, J. F., 1978. *Astrophys. J.*, **224,** 132.
Ciardullo, R., Ford, H., Bartko, F. & Harms, R., 1983. *Astrophys. J.*, **273,** 24.
Cowie, L. L., Hu, E. M., Jenkins, E. B. & York, D. G., 1983. *Astrophys. J.*, **272,** 29.
Crawford, C. S. & Fabian, A. C., 1992. *Mon. Not. R. astr. Soc.*, in press.
Daines, S. J., Fabian, A. C. & Thomas, P. A., 1992. *Mon. Not. R. astr. Soc.*, submitted.
Donahue, M. & Voit, G. M., 1991. *Astrophys. J.*, **381,** 361.
Donahue, M., Stocke, J. T. & Gioia, I. M., 1992. *Astrophys. J.*, **385,** 49.
Edge, A. C., Stewart, G. C. & Fabian, A. C., 1992. *Mon. Not. R. astr. Soc.*, **255,** 431.

Edge, A. C., Stewart, G. C., Fabian, A. C. & Arnaud, K. A., 1990. *Mon. Not. R. astr. Soc.,* **245,** 559.
Fabian, A. C. & Daines, S. J., 1991. *Mon. Not. R. astr. Soc.,* **252,** 17P.
Fabian, A. C., Nulsen, P. E. J. & Canizares, C. R., 1991. *Astr. Astrophys Rev.,* **2,** 191.
Gioia, I., Maccacaro, T., Schild, R., Wolter, A., Stocke, J., Morris, S. & Henry, J. P., 1990. *Astrophys. J. Suppl.,* **72,** 567.
Gregory, P. C. & Condon, J. J., 1991. *Astrophys. J. Suppl.,* **75,** 1011.
Heckman, T. M., Baum, S. A., van Breugel, W. J. M. & McCarthy, P., 1989. *Astrophys. J.,* **338,** 48.
Hill, J. M., Hintzen, P., Oegerle, W. R., Romanishin, W., Lesser, M. P., Eisenhamer, J. D. & Batuski, D. J., 1988. *Astrophys. J. Lett.,* **332,** L23.
Holtzman, J. A. *et al.,* 1992. *Astr. J.,* **103,** 691.
Howarth, I. D., 1983. *Mon. Not. R. astr. Soc.,* **203,** 301.
Johnstone, R. M. & Fabian, A. C., 1988. *Mon. Not. R. astr. Soc.,* **233,** 581.
Johnstone, R. M., Fabian, A. C. & Nulsen, P. E. J., 1987. *Mon. Not. R. astr. Soc.,* **224,** 75 (JFN87).
Kent, S. M. & Sargent, W. L. W., 1979. *Astrophys. J.,* **230,** 667.
Kristian, J., Sandage, A. & Westphal, J. A., 1978. *Astrophys. J.,* **221,** 383.
Kurucz, R. L., 1979. *Astrophys. J. Suppl.,* **40,** 1.
Lahav, O., Edge, A. C., Fabian, A. C. & Putney, A., 1989. *Mon. Not. R. astr. Soc.,* **238,** 881.
Lucey, J. R., 1983. *Mon. Not. R. astr. Soc.,* **204,** 33.
Mason, K. A., Spinrad, H., Bowyer, S., Reichert, G. & Stauffer, J., 1981. *Astr. J.,* **86,** 803.
McGilchrist, M. M., Baldwin, J. E., Riley, J. M., Titterington, D. J., Waldram, E. M. & Warner, P. J., 1990. *Mon. Not. R. astr. Soc.,* **246,** 110.
McHardy, I. M., Lawrence, A., Pye, J. P. & Pounds, K. A., 1981. *Mon. Not. R. astr. Soc.,* **197,** 893.
McNamara, B. R. & O'Connell, R. W., 1989. *Astr. J.,* **98,** 2018.
Moshir, M. *et al.,* 1989. *Explanatory Supplement to the IRAS Faint Source Survey,* IPAC preprint 44.
Mukai, K., 1990. *Publs astr. Soc. Pacif.,* **102,** 183.
Osterbrock, D. E., 1989. *Astrophysics of Gaseous Nebulae and Active Galactic Nuclei,* University Science Books, Mill Valley, USA.
Pesce, J. E., Fabian, A. C., Edge, A. C. & Johnstone, R. M., 1990. *Mon. Not. R. astr. Soc.,* **244,** 58.
Piccinotti, G., Mushotzky, R. F., Boldt, E. A., Holt, S. S., Marshall, F., Serlemitsos, P. J. & Shafer, R. A., 1982. *Astrophys. J.,* **253,** 485.
Raymond, J. C. & Smith, B. W., 1977. *Astrophys. J. Suppl.,* **35,** 419.
Robinson, A., Binette, L., Fosbury, R. A. E. & Tadhunter, C. N., 1987. *Mon. Not. R. astr. Soc.,* **227,** 97.
Romanishin, W., 1988. *Astrophys. J. Lett.,* **323,** L113.
Rubin, V. C., Ford, W. K., Jr, Peterson, C. J. & Oort, J. H., 1977. *Astrophys. J.,* **211,** 693.
Sandage, A., Kristian, J. & Westphal, J. A., 1976. *Astrophys. J.,* **205,** 688.
Sarazin, C. L., 1988. *X-ray emission from clusters of galaxies,* Cambridge University Press, Cambridge.
Seaton, M. J., 1979. *Mon. Not. R. astr. Soc.,* **187,** 75P.
Stark, A. A., Gammie, C. F., Wilson, R. W., Bally, J., Linke, R. A., Heiles, C. & Hurwitz, M., 1992. *Astrophys. J. Suppl.,* **79,** 77.
Sutherland, W., 1988. *Mon. Not. R. astr. Soc.,* **234,** 159.
Tonry, J. & Davis, M., 1979. *Astr. J.,* **84,** 1511.
Voges, W., 1992. In: *Proc. Second Conf. on Digital Optical Sky Surveys,* ed. MacGillivray, H. M., Edinburgh.
Warwick, R. S., Marshall, N., Fraser, G. W., Watson, M. G., Lawrence, A., Page, C. G., Pounds, K. A., Ricketts, M. J., Sims, M. R. & Smith, A., 1981. *Mon. Not. R. astr. Soc.,* **197,** 865.
White, D. A., Fabian, A. C., Johnstone, R. M., Mushotzky, R. F. & Arnaud, K. A., 1991. *Mon. Not. R. astr. Soc.,* **252,** 72.
Zabludoff, A. I., Huchra, J. P. & Geller, M. J., 1990. *Astrophys. J. Suppl.,* **74,** 1.